# Lagrangian 3D particle tracking for multi-pulse systems: performance assessment and application of Shake-The-Box

M. Novara[1,*], D. Schanz[1], S.Gesemann[1], K. Lynch[2], A. Schröder[1]
1: Institute of Aerodynamics and Flow Technology, German Aerospace Center, Germany
2: LaVision GmbH, Göttingen, Germany
* Correspondent author: matteo.novara@dlr.de

**Keywords**: 3D particle tracking, Shake-The-Box, multi-pulse, Lagrangian acceleration

ABSTRACT

The performances of the Shake-The-Box (STB) 3D particle tracking algorithm applied to images obtained from multi-pulse acquisition systems are investigated in the present study. Two synthetic experiments have been analyzed in order to assess the effects of experimental and processing parameters on the accuracy of the particle position, velocity and material acceleration measured by STB.

Results from the isotropic turbulence DNS simulation of the Johns Hopkins Turbulent Database are used to generate synthetic images where two four-camera 3D imaging systems are simulated to produce four-pulse time-resolved sequences; the delay between the four realizations is kept constant to deliver a maximum particle displacement of approximately 9 $px$. Several particle image densities are considered; real imaging effects have been simulated adding random noise to the particle images. The results show the capability of the iterative STB technique to progressively increase the number of successfully tracked particles even at high seeding densities; the beneficial effect of a more accurate reconstruction of the particle field is reflected in the lower errors in terms of particle position and velocity attained by further STB iterations.

In order to investigate the feasibility of material acceleration measurement with multi-pulse systems, a synthetic experiment from a ZDES simulation of an axisymmetric base flow at Mach 0.7 is considered, where the four pulses are unevenly separated in time in order to increase the measurement dynamic range. A seeding density typical of tomographic PIV experiments is applied (0.05 $ppp$, particles per pixel); the effect of image noise is also considered. Results show that the iterative STB processing is able to retrieve most of the actual particle tracks; the values of the estimated velocity and acceleration dynamic ranges are comparable to those obtained with STB in the time-resolved domain, opening the possibility of measuring material acceleration (and pressure) for high speed flows by means of multi-pulse acquisition systems.

Furthermore, a particle-based cross-correlation method is introduced here to obtain instantaneous velocity fields on a regular grid directly from the particle distributions reconstructed by IPR, therefore avoiding the computationally intensive discretization of the domain in voxel elements. The Particle-Space Correlation approach proved suitable to estimate 3D velocity fields to be used as a predictor during the tracking phase of the iterative STB technique.

## 1. Introduction

The recent introduction of the Shake-The-Box 3D particle tracking technique (Schanz et al 2013, 2016) opened the possibility to perform accurate Lagrangian particle tracking at seeding densities typical and exceeding those applied for tomographic PIV experiments (Tomo-PIV, Elsinga et al 2006). The method makes use of the particle based Iterative Particle Reconstruction technique (IPR, Wieneke 2013) to initialize particle tracks over a few recordings (typically four). Subsequently, the concept of particle *prediction* is introduced, where the position of tracked particles at following time instants is extrapolated from the initialized tracks; the predicted particle location is then corrected by means of the IPR image matching technique, referred to as *shaking*. As a consequence, the full IPR reconstruction is needed only during the initialization phase, which largely reduces the computational costs of the processing technique.

The STB technique takes advantage of time-resolved sequences to produce accurate Lagrangian particle tracks nearly free of *ghost particles*, typically not coherent with the flow motion over long time sequences (Elsinga et al 2011). Furthermore, the particle locations along the trajectories can be fitted in order to reduce the random particle position error introduced during reconstruction and to analytically evaluate velocity and material acceleration.

The measurement of the material acceleration is of particular interest for many industrial and engineering applications as it can be used to determine the instantaneous pressure field via the momentum equation (van Oudheusden 2013, Huhn et al 2015).

Due to current hardware limitations in terms of maximum acquisition frequency, time-resolved sequences suitable for STB processing can be obtained only for relatively low flow speeds (typically lower than 10 $m/s$). When higher speeds are attained, multi-pulse acquisition systems have been proposed; multiple imaging and illumination systems are operated in a staggered fashion in time to deliver short sequences of time resolved recordings. Unlike for high repetitions rate lasers, the time separation between the pulses can be freely adjusted down to few microseconds; as a consequence multi-pulse systems are suitable for the investigation of high speed flows, up to the transonic and supersonic regimes.

Recently multi-pulse investigations have been successfully performed by Schröder et al (2013) and Lynch and Scarano (2014), where four-pulses sequences have been recorded and processed by means of voxel-based tomographic reconstruction and cross-correlation techniques typical of Tomo-PIV.

In order to avoid the signal modulation introduced by the finite size of the interrogation volumes (particularly severe in strong shear regions and in the proximity of interfaces and walls - Kähler et al 2012a, 2012b) a novel STB approach for multi-pulse sequences has been proposed by

Novara et al (2015). To compensate for the lack of a large number of time-resolved realizations the method makes use of an iterative strategy where the sequential application of IPR and particle tracking is used to progressively reduce the complexity of the object to be reconstructed (i.e. the image seeding density of the images) and increase the number of successfully retrieved particle tracks.

The iterative STB technique has been applied to data from a multi-pulse turbulent boundary layer with adverse pressure gradient investigation in air at $36\ m/s$; approximately 80,000 tracks are identified for each instantaneous four-pulse sequence within the $50\times90\times8\ mm^3$ domain (along the stream-wise, wall normal and span-wise direction respectively).

Given the relatively high seeding density, the STB results have been interpolated onto a regular grid by means of a system of cubic b-splines (Gesemann 2016) and used for the visualization of instantaneous flow structures. On the other hand, the availability of single particle tracks enabled the evaluation of highly spatially resolved mean and fluctuating velocity profiles by mean of ensemble averaging.

The high spatial resolution offered by the tracking approach, combined with the relatively large investigated domain, allows for the measurement of a wide range of spatial scales; the boundary layer statistics obtained with STB compared well with the results obtained by long-range micro-PTV in the near wall region and with those from planar PIV in the outer region of the boundary layer (Novara et al 2015).

On the other hand, a quantitative assessment of the performances of the iterative STB approach for multi-pulse data is not yet available, which motivates the present study. The effects of experimental and processing parameters such as seeding density, image noise, time delay between pulses, number of iterations among others are characterized here by means of the analysis of two synthetic experiments, where the availability of the ground-truth allows for the quantification of the accuracy of the STB results.

## 2. Iterative Shake-The-Box approach

Several techniques have been proposed in order to separate the four pulses generated by a dual double-pulse laser illumination system. Lynch and Scarano (2014) suggested the use of three independent imaging systems, two operating in single-frame mode to acquire the first two pulses and the third recording in double-frame fashion for the last two realizations.

On the other hand, a method based on the use of polarized light has been presented by Kähler and Kompenhans (2000) and Schröder et al (2013) where the lasers emit light with two

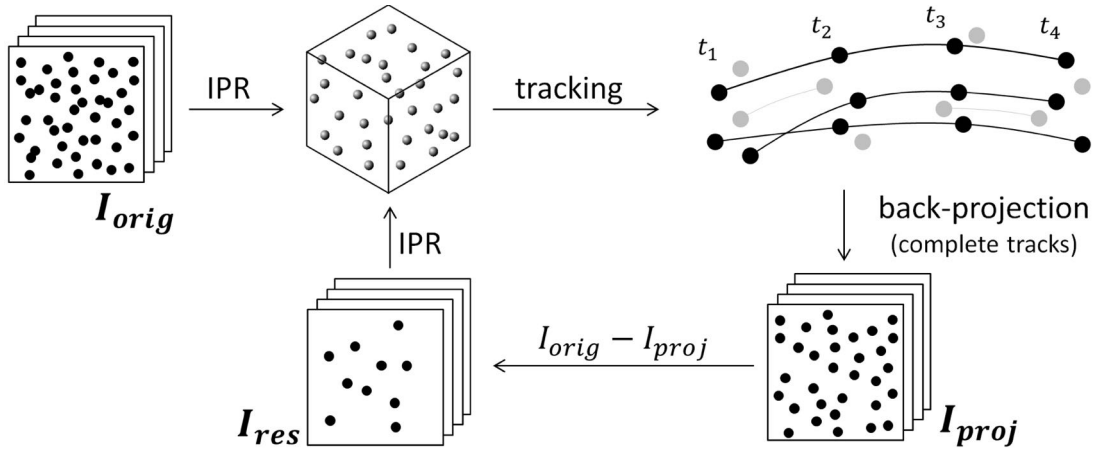


Figure 1. sketch of iterative STB processing for multi-pulse sequences.

polarization states rotated by $90^o$; two imaging systems operate in double-frame mode, where cameras are equipped with polarizing filters to separate the four pulses and avoid double-exposed particle images. The investigation of the different pulse separation strategies goes beyond the scope of the present work and it is devoted to a future study.

The iterative processing strategy for STB applied to multi-pulse data is presented in Figure 1; four pulses separated by a constant time delay $\Delta t$ are considered here $(t_1, t_2, t_3, t_4)$. The recorded images $(I_{orig})$ are reconstructed for each pulse by means of IPR; the IPR processing parameters (number of triangulations $m$, triangulations with a reduced camera system $n$, shaking iterations $k$, allowed triangulation error and intensity threshold for 2D peaks detection) are chosen based on the image quality and seeding density.

After the IPR reconstruction, particle tracking is performed across the four-pulse sequence; starting from the second pulse, around each particle a search area is defined to identify possible partners at the previous time instant and track candidates are built. The choice of the search radius depends on the estimated particle displacement or a on the estimated accuracy of a predictor for the velocity field, if available.

A linear fit is applied to the particle locations along the track candidates and a residual from the fit is computed as the mean quadratic distance between the reconstructed and fitted particle positions. Among track candidates that share at least one particle, the one with the lower residual value is retained while the others are discarded. Furthermore, a threshold value for the residual is chosen; all candidates exhibiting a residual larger than the threshold are rejected.

After the tracking step is performed, particles that could not be tracked over the complete four-pulse sequence are rejected (gray dots in Figure 1-top-right).

As most of *ghost particles* tend to be inconsistent with the flow motion and fail to produce coherent tracks (Elsinga et al 2011), this step ensures that most of retained tracks (black dots) refer to actual particles. Furthermore, when two independent imaging systems are employed, the chance of producing *ghost tracks* is drastically reduced (Discetti et al 2013, Novara et al 2015). As this is typically the case for multi-pulse experiments, the particle field obtained after rejecting incomplete particle tracks can be considered as nearly free of *ghosts*.

The retained particles are then back-projected onto the image plane to form projected images ($I_{proj}$); these are subtracted from the original recordings to obtain residual images ($I_{res}$).

These steps constitute a single STB iteration; particles images which have not been reconstructed by IPR (e.g. due to particle image overlapping situations) or failed to be matched during tracking (e.g. due to inaccurate predictor or inadequate search radius) remain in the residual images.

Residual images are reconstructed by IPR to perform a further STB iteration; these images typically exhibit a lower image seeding density ($ppp$) therefore offering a less complex reconstruction and tracking problem.

As a consequence, the iterative application of STB is expected to enable the recovery of previously undetected particles, potentially overcoming the limitations in terms of seeding density imposed by the use of particle reconstruction alone (typically 0.05 $ppp$ for both IPR and MART, Multiplicative Algebraic Reconstruction Technique – Herman and Lent 1976).

**3. Performance assessment based on synthetic experiments**

Experimental and processing parameters affect the accuracy of the particle position, velocity and acceleration measured by STB. In order to quantify the performances of the technique, synthetic multi-pulse experiments have been analyzed where experimental conditions can be controlled and reference data for the particle and velocity fields are available.

Results from numerical simulations of isotropic turbulence and of a transonic base flow are used to generate images from virtual acquisition systems operating in multi-pulse mode. Concerning the first case, four pulses are generated with a constant time separation while, in the second case, a larger separation is adopted between the second and third pulse to increase the dynamic range and allow a more accurate measurement of the material acceleration. In both cases ideal particle images are analyzed as well as noisy ones, where real imaging effects have been included.

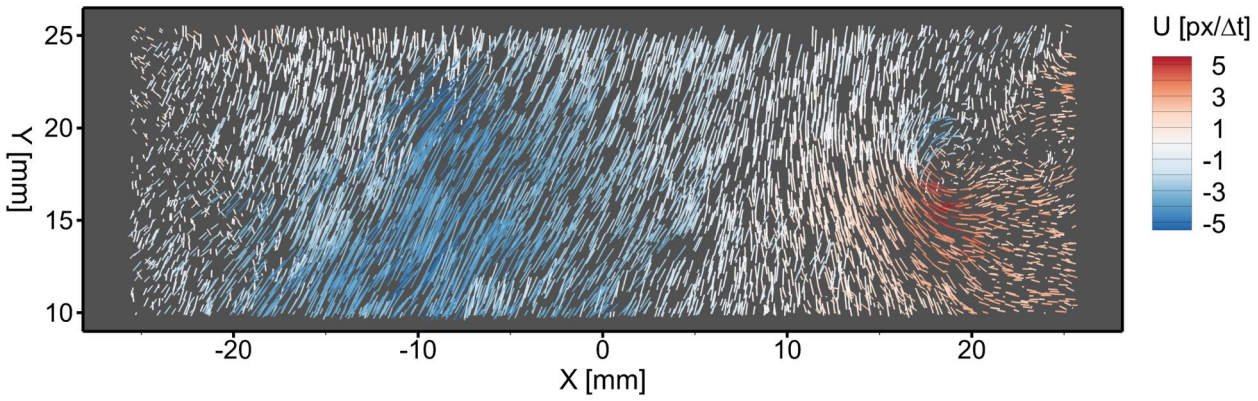


Figure 2. Reference four-pulse tracks within a sub-region of the investigated domain ($-2.5 < Z < 2.5\ mm$) visualized by plotting the velocity vector at each particle location; tracks are color-coded by the value of the $X$ velocity component.

Furthermore, for the isotropic turbulence case, several seeding densities have been considered to investigate the capability of the iterative process in delivering instantaneous high spatial resolution particle track fields. A detailed description of the test cases and of the processing parameters and results of the STB is presented in the remainder of this section.

**Isotropic turbulence case**

A region within the domain of the DNS forced isotropic turbulence case of the Johns Hopkins turbulent database (Cao and Chen 1999) is chosen to produce a volume of 51.2×51.2×12.8 $mm^3$ along the $X, Y$ and $Z$ directions respectively. The digital resolution is 20 $px/mm$; a constant time separation ($\Delta t$) between the four pulses is chosen in order to have a maximum particle displacement between subsequent pulses of approximately 9 $px$.

Particles are randomly distributed in the 3D space and blobs are generated via 3D Gaussian integration; camera images are produced using a pinhole camera model and 2D Gaussian integration as in Lynch and Scarano (2015). Ground-truth reference particle tracks (Figure 2) are produced along the four pulses integrating the velocity field from the DNS data by means of a second-order accurate trapezoidal method.

The size of the camera images is 1280×1280 $px$ and the particle diameter is 3 $px$; a Gaussian illumination profile along the $Z$ direction is assumed for the definition of the peak intensity.

Two imaging systems made of four cameras each ($N_c = 4$) are simulated to reproduce the multi-pulse acquisition strategy adopted by Schröder et al (2013) and by Novara et al (2015); the first system records pulses at $t_1, t_3$ while the second system acquire pulses at $t_2, t_4$.

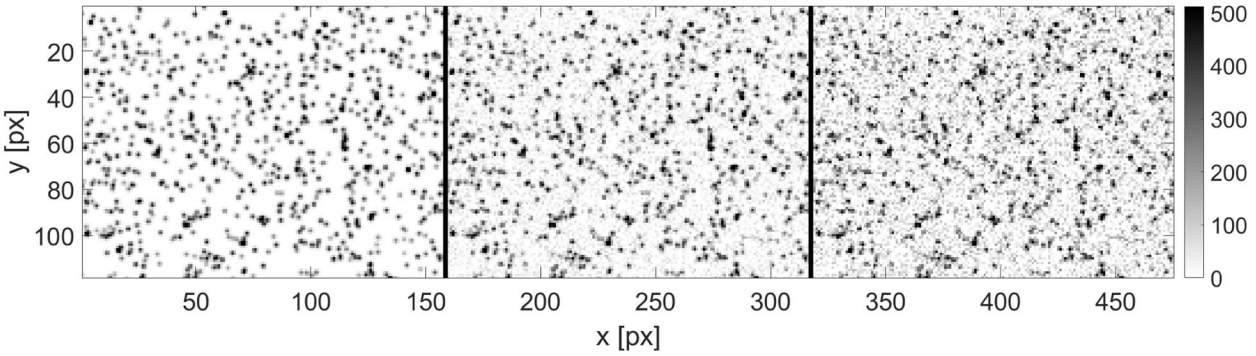


Figure 3. Details of camera images at $0.05\,ppp$ for different noise levels (from left to right: $\sigma = 0$, $\sigma = 0.1 \cdot \bar{I}_p$ and $\sigma = 0.2 \cdot \bar{I}_p$).

Cameras are positioned at the corners of a trapezoid, where the maximum aperture angle is $60^o$ and the minimum is $20^o$; the two systems are built in a symmetric configuration with respect to the imaged domain in order to ensure a similar reconstruction quality for each pulse.

The particle seeding density is varied between $0.25$ and $3$ particles per cubic millimeter corresponding to an effective imaged density of $0.01 \div 0.125\,ppp$. Given the size of the active portion of the camera image, slightly smaller than $1280\times1280\,px^2$, the number of actual particles ranges approximately between 6,000 and 100,000.

Following Schanz et al (2016), the effect of image noise is simulated by adding to each pixel a randomized intensity from a normal distribution with variance $\sigma$; four cases are investigated ranging from noise-free ideal particle images ($\sigma = 0$) to $\sigma = 0.2 \cdot \bar{I}_p$, where $\bar{I}_p = 380\,counts$ is the average imaged particle peak intensity. Details of the synthetic images are shown in Figure 3 for

Table 1. Processing parameters for STB

| | $\sigma = 0$ | $\sigma = 0.03 \cdot \bar{I}_p$ | $\sigma = 0.1 \cdot \bar{I}_p$ | $\sigma = 0.2 \cdot \bar{I}_p$ |
|---|---|---|---|---|
| triangulations with $N_c$ | 6 | 6 | 6 | 6 |
| triangulations with $N_{c-1}$ | 4 | 4 | 4 | 4 |
| shake iterations | 8 | 8 | 8 | 8 |
| shake width [px] | 0.1 | 0.1 | 0.1 | 0.1 |
| allowed triang. error [px] | 1 | 1 | 1 | 1 |
| 2D peaks int. threshold [counts] | 40 | 40 | 40 | 40 |
| 2D peaks used for triang. $\eta$ [%] | 50 | 50 | 20 | 15 |
| track search radius [px] | 3 | 3 | 3 | 3 |
| STB iterations | 15 | 15 | 15 | 15 |

three different noise levels. Volume Self Calibration (Wieneke 2008) is carried out in order to determine the optical Transfer Function of the particle images (Schanz et al 2013).

The main STB processing parameters are shown in Table 1; a smoothness threshold of $2\,px$ is employed to discard track candidates exhibiting high deviation with respect to a linear fit (typically $< 1\%$ of the total number of candidates).

With respect to what proposed by Schanz et al (2016), a different thresholding strategy is adopted here for the identification of the particle peaks onto the camera images. Instead of selecting a static threshold, a low threshold of $40\,counts$ is used (potentially within the image noise in case of real imaging effects) to list all possible 2D peaks; however, only the brightest peaks are considered for triangulation. The number of brightest peaks is determined as a percentage of the total number of detected peaks based on the value of $\eta$ (ranging from $50\%$ to $15\%$ for the present case). This approach results in a progressive reduction of the effective intensity threshold during the iterative STB process. A lower value of $\eta$ when dealing with noisy images results in a slower convergence rate in terms of detected tracks, but also ensures that the weaker, and potentially noisy peaks, are not taken into account for the first STB iterations when, particularly for the high seeding density case, the IPR reconstruction problem is more complex (higher $ppp$ onto the recorded and residual images).

When dealing with experimental images, where typically different cameras show different particle brightness, this strategy helps in balancing the number of detected peaks between the cameras without the aid of image intensity equalization via pre-processing.

The tracking process is carried out with the aid of a velocity predictor obtained sampling the ground-truth velocity field on a regular grid; a search radius of $3\,px$ around the predicted particle location is used to compensate for interpolation errors.

A Tomo-3D-PTV approach as proposed by Novara and Scarano (2013) is also applied; images are reconstructed by means of an in-house implementation of the SMART algorithm (Atkinson and Soria 2009) to produce $1200\times1200\times280\,vox^3$ objects (20 SMART iterations); DaVis 8.2.2 (LaVision GmbH) is used to identify 3D particle peaks above a $500\,counts$ intensity threshold (the intensity value differs from the imaged one as the values of the reconstructed voxels are scaled to the 16-bit unsigned integer range before storage). The same tracking algorithm used within the STB is used to track the particles from Tomo-PIV along the four pulses.

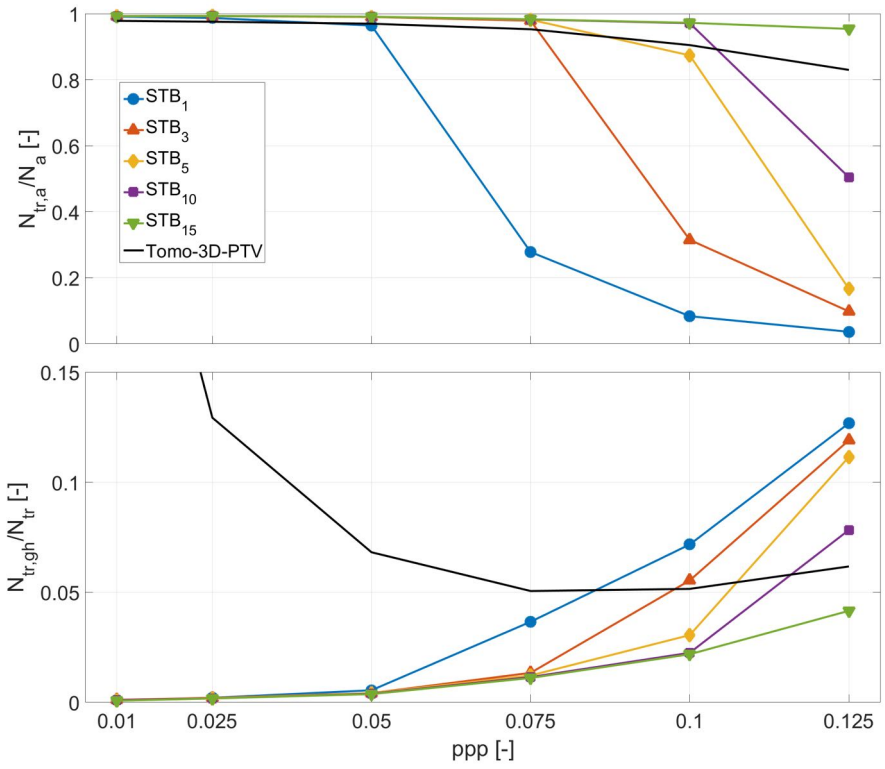


Figure 4. Results for the intermediate noise case ($\sigma = 0.1 \cdot \bar{I}_p$); *top*: fraction of tracked-actual ($N_{tr,a}$) with respect to the number of actual particles ($N_a$). *Bottom*: fraction of tracked *ghost* particles ($N_{tr,gh}$) with respect to the total number of tracked particles ($N_{tr}$).

A thorough comparison between STB and Tomo-3D-PTV, where more sophisticated algorithms for the tomographic approach could be applied (e.g. Motion Tracking Enhancement, MTE Novara et al 2010), goes beyond the scope of the present investigation; Tomo-3D-PTV is used here merely to provide a reference for the STB performances.

Following Schanz et al (2016), within the total number of tracked particles $N_{tr}$, the tracked–actual particles $N_{tr,a}$ are defined as the ones found within a distance of 1 $px$ from the reference particles. On the other hand, a tracked particle is considered as part of a *ghost track* when no actual reference particle is found in its vicinity ($N_{tr,gh}$). The ratio between the number of tracked–actual particles detected by STB and Tomo-3D-PTV and the number of reference particles is shown in Figure 4-top as a function of the seeding density; results refer to the intermediate noise case ($\sigma = 0.1 \cdot \bar{I}_p$). Several curves are plotted referring to the STB results at different iterations.

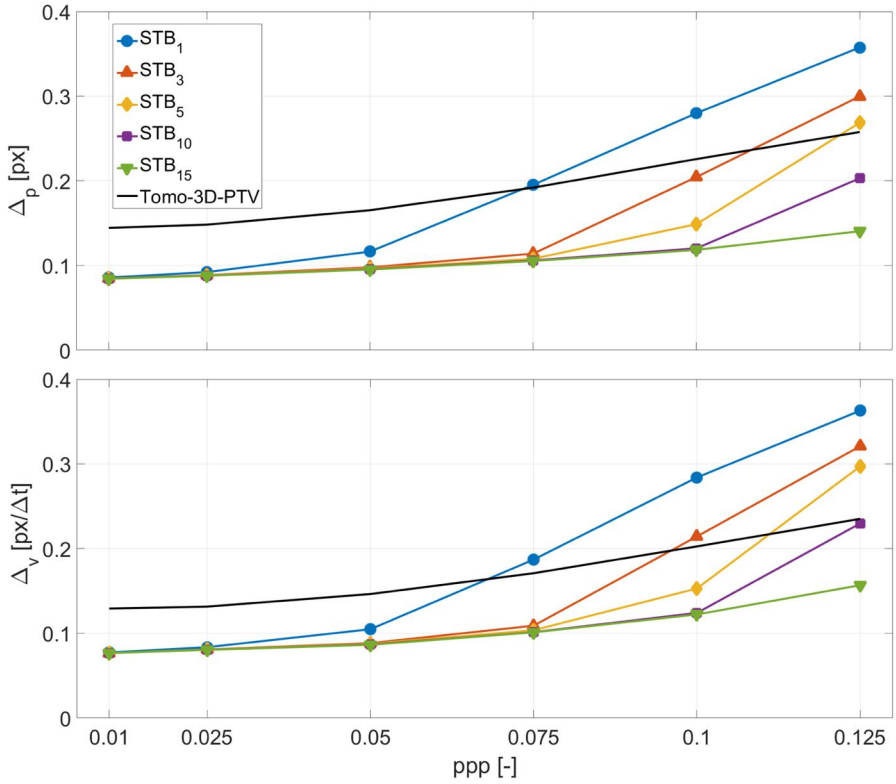


Figure 5. Results for the intermediate noise case ($\sigma = 0.1 \cdot \bar{I}_p$); *top*: average position error of tracked-actual particles. *Bottom*: average velocity error of tracked-actual particles.

A large number of iterations (15) has been performed here to assess the asymptotic behavior of the iterative technique. Given the seeding densities commonly encountered in real experimental applications, typically lower than 0.1 *ppp*, 5 iterations appear to be sufficient to ensure that most particles are identified.

It can be observed that even at high seeding density, the iterative STB strategy is able to recover almost the totality of actual particles. The challenge posed to the IPR reconstruction by the object complexity is evident when looking at the low number of particles tracked after the first STB iteration for $ppp > 0.05$.

The fact that the Tomo-3D-PTV approach consistently finds a lower number of tracks can be addressed to the choice of the intensity threshold level for peak identification in the reconstructed objects. On the other hand, when the ratio between the *ghost* and the total number of reconstructed tracks is considered, Figure 4-bottom, the impact of *ghost tracks* is stronger for the tomographic case, particularly at low *ppp* where the noisy peaks are dominant with respect to the number of actual particles.

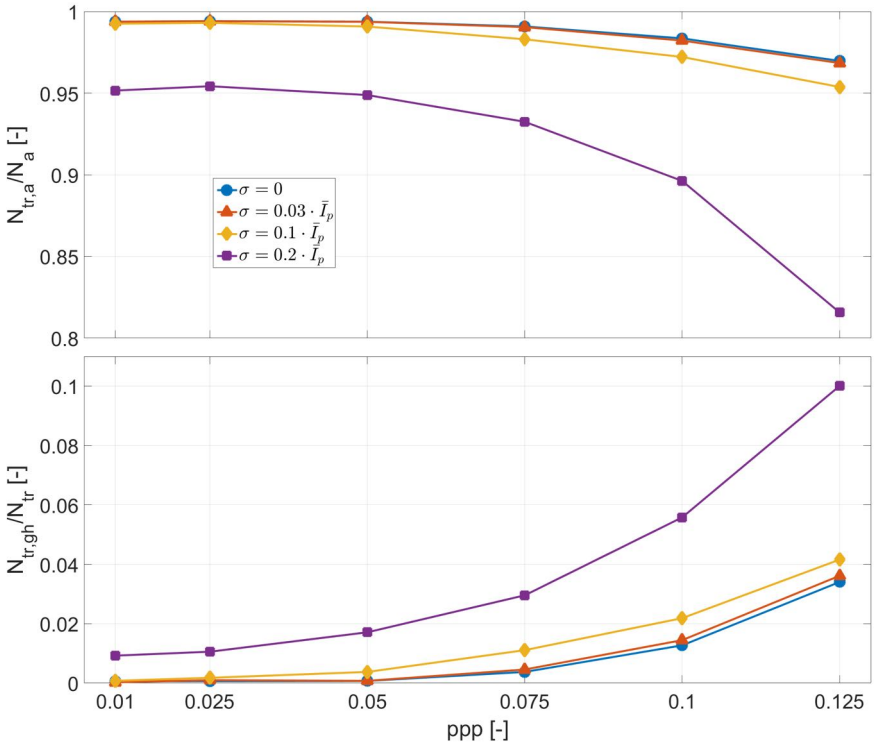


Figure 6. Results for converged STB (15 iterations); *top*: fraction of tracked-actual ($N_{tr,a}$) with respect to the number of actual particles ($N_a$). *Bottom*: fraction of tracked *ghost* particles ($N_{tr,gh}$) with respect to the total number of tracked particles ($N_{tr}$).

On the other hand the STB approach is able to limit the spurious tracks below 5% even for the 0.125 *ppp* case; these results confirm that the iterative STB is able to overcome the limitations in terms of seeding density of IPR alone (0.05 *ppp*, Wieneke 2013).

A second order polynomial fit is applied to the particle location along the track in each direction separately; particles are relocated to the fitted position and their velocity is evaluated from the fit. The average particle peak location ($\Delta_p$) and velocity ($\Delta_v$) errors are computed as:

$$\Delta_p = \frac{1}{N_{tr,a}} \sum_{1}^{N_{tr,a}} \left| \vec{x}_{tr,a} - \vec{x}_a \right| \qquad 1$$

$$\Delta_v = \frac{1}{N_{tr,a}} \sum_{1}^{N_{tr,a}} \left| \vec{v}_{tr,a} - \vec{v}_a \right|$$

The position and velocity average errors are shown for the different seeding density levels in Figure 5; the overall advantage provided by the IPR technique with respect to tomographic reconstruction is visible in terms of the particle peak location accuracy and it is reflected in the higher accuracy of the particle velocity estimation from STB. The progressive reduction of both

errors with further STB iterations is explained by the fact that the IPR accuracy improves as the number of reconstructed actual particles increases. In fact, the back-projected reconstructed objects better match the camera images, effectively aiding the image matching-based correction of the particle peak location.

The performances of STB when dealing with different image noise levels are presented in Figure 6 and Figure 7; results refer to the converged state of the iterative STB after 15 iterations. Even when strong image noise levels are present, the STB technique is able to correctly identify more than 80% of the actual tracks at a seeding density of 0.125 $ppp$. For seeding densities typical of experimental applications more than 90% actual particles are reconstructed. On the other hand the presence of ghost tracks is limited to 10% of the total number of tracks for the most challenging case where strong noise and high seeding density are combined.

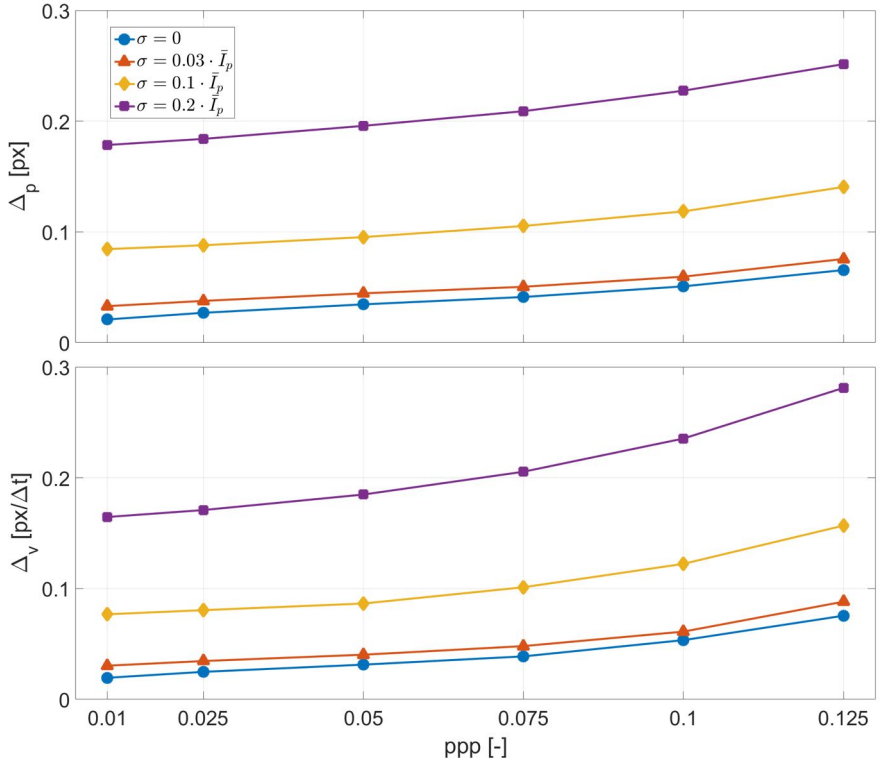


Figure 7. Results for converged STB (15 iterations): *top*: average position error of tracked-actual particles. *Bottom*: average velocity error of tracked-actual particles.

The performances of the method regarding position and velocity errors are shown in Figure 7; a maximum error of 0.1 $px$ and 0.1 $px/\Delta t$ for particle position and velocity respectively is found in most of the conditions likely to be encountered in real experiments ($ppp < 0.1$ and intermediate noise levels). The position error values well compare with the values indicated by Schanz et al

(2016); as expected, the limited observation time offered by the multi-pulse acquisition does not allow for a significant reduction of the measurement noise by means of track fitting as reported for the time-resolved case.

**Transonic base flow case**

Within the framework of the European FP-7 project NIOPLEX (http://nioplex.eu/), a synthetic experiment has been generated, among other test cases, in order to assess the suitability of multi-pulse data to extract instantaneous 3D pressure fields. As the measurement of the material acceleration is needed for the pressure gradient evaluation by means of the momentum equation, the Lagrangian particle tracking offered by the STB approach appears to be a suitable processing technique.

A more detailed description of the test cases and the techniques employed for pressure determination can be found in Blinde et al (2016), as well as a comparative analysis of the results. In the current study the application and performances of the STB technique only are discussed.

Results from a Zonal Detached Eddy Simulation (ZDES, Deck 2005, 2012) of a transonic flow over an axisymmetric step are used to produce synthetic particle images from a four-camera 3D imaging system.

The main body has a dimeter $(D)$ of $50\,mm$ and an afterbody of diameter $(d)$ of $20\,mm$; as a consequence, the step height is $15\,mm$. The flow has a Mach number of 0.7, resulting in a free stream velocity of $226\,m/s$ $(Re_D = 1.3 \cdot 10^6)$. The measurement domain of the synthetic experiments encompasses $60\times24\times4\,mm^3$ along the stream-wise $(X)$, wall-normal $(Y)$ and span-wise $(Z)$ directions respectively.

Tracer particles are randomly generated within the 3D domain in order to produce particle images with an imaged seeding density of approximately $0.05\,ppp$; particles are propagated based on the velocity field from the numerical simulation using an explicit Runge-Kutta method.

Particle images are generated on virtual camera sensors of $1624\times800\,px^2$, a pixel pitch of $4.4\,\mu m$ and equipped with lenses having $75\,mm$ focal length; a pinhole camera model and 2D Gaussian integration are used to project the particles onto the image plane. The digital resolution is $22.9\,px/mm$. The four cameras are placed in cross configuration with yaw and pitch angles of $\pm30^o$.

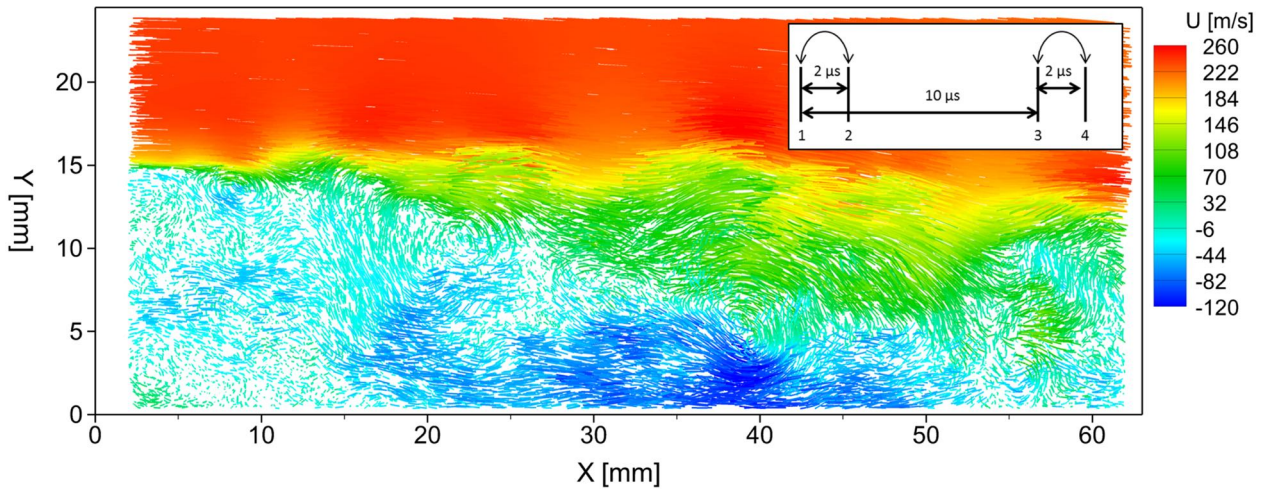


Figure 8. Approximately 26,000 ground-truth reference tracks within the investigated domain; tracks are color-coded by the stream-wise velocity component; the four-pulse timing sequence is depicted in the top-right corner.

Ideal particle images having an image diameter of 2 $px$ and a peak intensity of 512 $counts$ are generated as well as noisy particle images to simulate experimental imaging conditions.

For the latter case a particle imaged diameter of 2.5 $px$ is chosen along with a lower nominal peak intensity of 342 $counts$. The physical size of the particle tracers is chosen from a Gaussian distribution with a mean value of 400 $nm$ and a standard deviation of 100 $nm$, resulting in particle peak intensity ranging within $21 \div 1731$ $counts$. Camera shot noise is added to the particle images; a random value from a Poisson distribution with mean value equal to the intensity of the noise-free pixel is added to each pixel. Moreover, thermal noise is also simulated adding random intensity values from a Poisson distribution with constant mean value across the image. As a consequence, image preprocessing is applied for the noisy image case, where a constant value representative of the mean thermal noise is subtracted.

A series of 21 statistically independent instantaneous four-pulse sequences is generated for both cases; an example of the instantaneous ground-truth reference track field is shown in Figure 8 where the particle tracks have been color-coded based on the value of the stream-wise velocity component. The origin of the coordinate system is placed at the lower corner of the step.

The four-pulse image acquisition timing sequence is depicted in Figure 8; an uneven spacing is applied in order to extend the measurement dynamic range and allow for the evaluation of more accurate particle material acceleration. A short time delay of 2 $\mu s$ separates the first and last two pulses while a larger separation of 8 $\mu s$ is present between the second and third pulse (approximately 10 $px$ and 44 $px$ maximum particle displacement respectively). A calibration for the Optical Transfer Function is obtained together with Volume Self Calibration.

For each time instant two velocity fields to be used as predictors for particle tracking ($\vec{v}_{p_{12}}$ and $\vec{v}_{p_{34}}$) are obtained by means of the Particle-Space Correlation technique (see appendix) applied to the IPR reconstructed particles of pulses 1,2 and 3,4 respectively (with a final cross-correlation window of $24^3$ $vox^3$).

The STB is applied following the iterative strategy presented in section 2. Nevertheless, an adapted tracking strategy is applied here to cope with the uneven time separation between the pulses. A sketch of the particle tracks definition is shown in Figure 9.

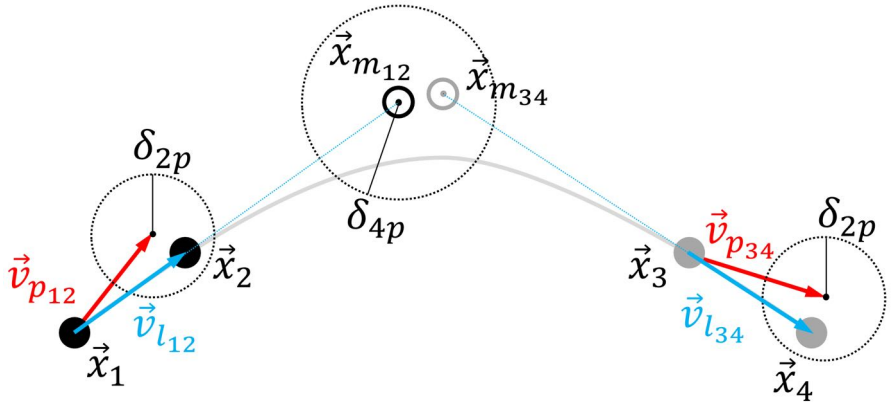


Figure 9. Sketch of track candidate identification for unevenly spaced pulses.

After IPR reconstruction of the four time instants, a partner search between the particles from pulse $t_1$ and $t_2$ is performed; the location of each particle from $t_1$ is predicted at time $t_2$ making use of the predictor field ($\vec{v}_{p_{12}}$). A search area is centered at the predicted location having radius equal to $\delta_{2p}$; if at least one particle from $t_2$ is found within the search area, a two-pulse track is created connecting the particle at $t_1$ with the closest particle at $t_2$. The same procedure is applied to create two-pulse tracks between the third and fourth pulses.

For each two-pulse track identified across the first two pulses, a prediction of the particle location at the mid-point of the four pulse sequence ($\vec{x}_{m_{12}}$ in Figure 9) is obtained by extrapolation of the velocity obtained from the linear interpolation of the particle positions ($\vec{v}_{l_{12}}$). The same is done to determine the midpoint $\vec{x}_{m_{34}}$ locations from pulses 3 and 4.

When the predicted mid-point locations of two short tracks from pulses 1,2 and 3,4 are found within a distance of $\delta_{4p}$, a complete four-pulse track is built. A second order polynomial is fitted to the four particle locations in time and an average residual from the fit is computed as:

$$\varepsilon_{fit} = \frac{1}{4}\sum_{i=1}^{4} |\vec{x}_i - \vec{x}_{i,fit}| \qquad 2$$

If the average residual is larger than a threshold value ($\varepsilon_{fit}^*$), the track candidate is discarded. In case two or more track candidates share the same particles, the candidate with the lowest average residual value is retained while the others are discarded.

As shown in Figure 1, only complete four-pulse tracks are retained in order to produce the projected and residual images to be used as input for further STB iterations.

An optimized track-fit based on a system of cubic b-splines (Gesemann 2016) is applied to the four-pulse tracks in order to analytically evaluate the particle velocity and acceleration; a normalized cut-off frequency ($f_{co}$) is applied to reduce the high frequency content introduced by measurement noise in the particle location. While for time-resolved measurements the cut-off frequency can be determined via spectral analysis of the unfitted tracks (Schanz et al 2016), for the multi-pulse case the choice is dictated by the imaging conditions (e.g. noise level).

After a significant number of tracks are identified by initial STB iterations, a validation of new tracks can be applied based on neighboring tracks acceleration to exclude potential outliers. For each new track the closest $N_{val}$ neighbors are identified and the mean and standard deviation of the acceleration magnitude evaluated ($\bar{a}$ and $a_{std}$). The difference between the acceleration of the current particle ($a_p$) and the average acceleration is computed as:

Table 2. Processing parameters for STB; when a different parameter value is chosen at each STB iteration, multiple values are given, separated by a comma.

| | clean | noisy |
|---|---|---|
| triangulations with $N_c$ | 4 | 4 |
| triangulations with $N_{c-1}$ | 2 | 2 |
| shake iterations | 5 | 5 |
| shake width [px] | 0.1 | 0.1 |
| allowed triangulation error [px] | 0.6 | 1.1 |
| 2D peaks int. threshold [counts] | 20 | 20 |
| 2D peaks used for triang. $\eta$ [%] | 100 | 10, 10, 10, 10, 20 |
| search radius two-pulse tracks, $\delta_{2p}$ [px] | 0.5, 2.5, 4 | 0.5, 1, 3, 5, 3.5 |
| search radius four-pulse tracks, $\delta_{4p}$ [px] | 1, 2, 3 | 2, 2, 3, 4, 5 |
| maximum residual from fit (2nd poly), $\varepsilon_{fit}^*$ [px] | 0.08, 0.25, 0.35 | 0.2, 0.25, 0.25, 0.35, 0.35 |
| num. neighbors for acc. validation, $N_{val}$ ($N_{val}^*$) | 0, 50, 50 (50) | 0, 0, 50, 50, 50 (50) |
| acc. validation factor, $C_{val}$($C_{val}^*$) | 0, 10, 8 (6) | 0, 0, 3, 5, 5 (4) |
| track-fit cut-off frequency, $f_{co}$ | 0.35 | 0.15 |
| STB iterations | 3 | 5 |

$$\Delta_{a_p} = a_p - \bar{a} \qquad 3$$

If $\Delta_{a_p} > C_{val} \cdot a_{std}$ for at least one particle along the four pulses, the track is rejected.

After the last STB iteration is performed, a final validation step is applied possibly using different validation parameters, namely $N_{val}^*$ and $C_{val}^*$. The maximum number of rejected tracks due to validation is less than 2% both for the ideal images and noisy case.

The main STB processing parameters are presented in Table 2 for both test cases.

For the clean case, all peaks above an intensity threshold of 20 $counts$ are considered for triangulation; on the other hand, only a small portion of the detected peaks is triangulated for the noisy case ($\eta = 10 \div 20\%$). This strategy allows to progressively reducing the effective intensity threshold at further iterations; as a consequence the detrimental effect of noisy peaks is avoided in the initial phase of STB, particularly critical due to the high image density exhibited by the recorded and residual camera images.

Concerning the particle tracking, the low values of the search radiuses and of the maximum deviation from the 2nd order polynomial fit chosen for the first STB iterations ensure that only the most reliable tracks are identified. After these particles have been subtracted from the recorded images, more challenging tracks (e.g. exhibiting high noise or high accelerations) can be identified by relaxing the partner search and track smoothness parameters.

The performances of STB are evaluated at the mid-point of the tracks where the maximum accuracy of the track-fit is attained; results are obtained averaging across the 21 time instants.

Unlike for the reference particle position and velocity, a ground-truth value for the material acceleration is not directly available from the ZDES simulation results. As a consequence, the reference material acceleration is obtained applying a fit to the ground-truth particle locations. A system of cubic b-splines is used to fit both the particle position and velocity along the track; the reference material acceleration is derived analytically from the fit.

For each reference particle, a search area having 1 $px$ radius is located at the peak position; if at least one STB particle is found within the search area, the particle is considered as detected and the errors in terms of positon, velocity and acceleration are evaluated as:

$$\Delta_p = \frac{1}{N_{tr,a}} \sum_{1}^{N_{tr,a}} \left|\vec{x}_{tr,a} - \vec{x}_a\right| \qquad rms_p = \sqrt{\frac{1}{N_{tr,a}} \sum_{1}^{N_{tr,a}} \left(\vec{x}_{tr,a} - \vec{x}_a\right)^2}$$

$$\Delta_v = \frac{1}{N_{tr,a}} \sum_{1}^{N_{tr,a}} \left|\vec{v}_{tr,a} - \vec{v}_a\right| \qquad rms_v = \sqrt{\frac{1}{N_{tr,a}} \sum_{1}^{N_{tr,a}} \left(\vec{v}_{tr,a} - \vec{v}_a\right)^2} \qquad 4$$

$$\Delta_a = \frac{1}{N_{tr,a}} \sum_{1}^{N_{tr,a}} |\vec{a}_{tr,a} - \vec{a}_a| \qquad rms_a = \sqrt{\frac{1}{N_{tr,a}} \sum_{1}^{N_{tr,a}} \left(\vec{a}_{tr,a} - \vec{a}_a\right)^2}$$

When no particle reconstructed from STB is found in the vicinity of the reference particle, this is listed as undetected. On the other hand, the number of *ghost* particles is computed searching for reference particles in the area surrounding each reconstructed particle; when no actual particle is found the peak is considered as a *ghost*. Results refer only to *ghost* particles that produced a four-pulse track; the total number of *ghosts* produced for each pulse by IPR alone is larger than the number of tracked *ghosts*.

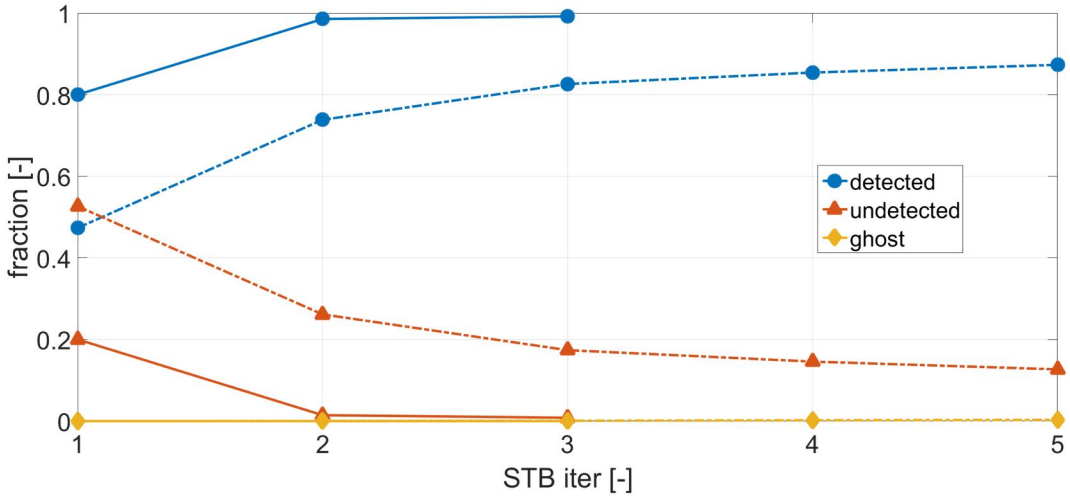


Figure 10. Fraction of reconstructed particles by STB with respect to the number of ground-truth reference particles attained at different STB iterations. Solid lines refer to the clean case, while dotted lines to the noisy case.

The fraction of detected, undetected and *ghost* particles with respect to the number of actual reference four-pulse tracks is shown in Figure 10 for both the clean and noisy case. As expected, the number of detected particles increases with further STB iteration. For the clean case a converged state is reached after two iterations only, while, for the noisy case, five iterations appear to be not completely sufficient to reach an asymptotic condition.

Approximately 99% and 88% of reference particles are identified by STB for the clean and noise case respectively. For both cases, the fraction of tracked ghost particles is lower than 1%; despite the fact that one imaging system only is used, the relatively large time separation between the pulses ensures that most of ghost particles do not follow coherent trajectories.

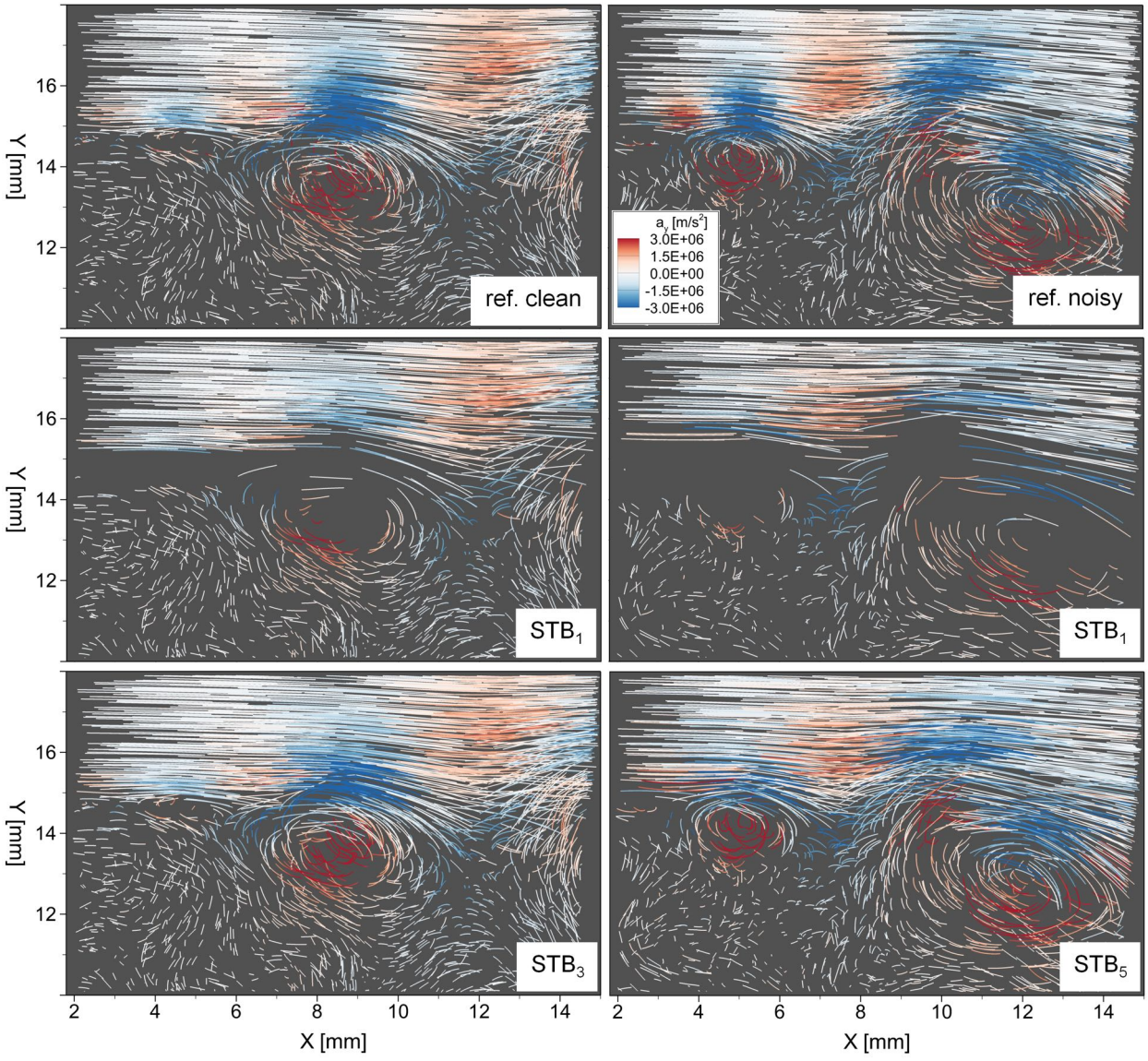


Figure 11. Detail of instantaneous reference and STB (first and last iteration) tracks for the clean (left) and noisy case (right); tracks are color-coded with the value of material acceleration along the $Y$ axis ($a_y$).

Examples of instantaneous reference tracks for both cases are shown in Figure 11 together with the STB results for the first and last iteration; tracks are color-coded with the value of the material acceleration along the $Y$ axis. Consistently with the tracking parameters settings shown in Table 2, the tracks exhibiting the highest acceleration values are not retrieved at the first iterations.

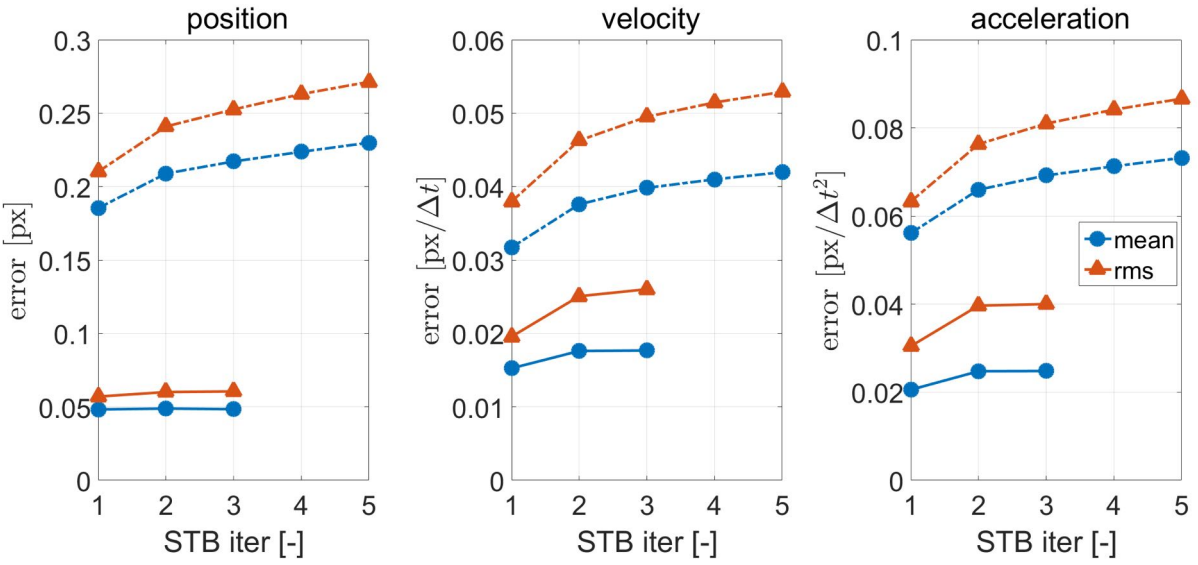


Figure 12. Position, velocity and material acceleration errors for different STB iterations (mean and root-mean-square in blue and orange respectively); solid lines refer to the clean case while dotted lines to the noisy case.

As the number of detected particles increases with the iterations, high curvature trajectories are identified where the accuracy of the track-fit approach is affected (i.e. due to the non-optimal choice of the cut-off frequency parameter in high acceleration regions). This justifies the behavior of the mean and rms position, velocity and material acceleration error shown in Figure 12, where both values increase with the number of iterations.

As expected, the errors relative to the noisy case are consistently higher than the ones for the clean case.

Following Adrian (1997), the dynamic velocity (DVR) range of the measurement can be estimated as the ratio between the maximum velocity magnitude within the investigated domain and the velocity rms error; the same approach can be followed to compute the dynamic

Table 3. Velocity and acceleration errors and dynamic ranges relative to the last STB iteration.

| | clean | noisy |
|---|---|---|
| $\Delta_v\ [px/\Delta t]$ | 0.018 | 0.042 |
| $rms_v\ [px/\Delta t]$ | 0.026 | 0.053 |
| DVR | 467 | 223 |
| $\Delta_a\ [px/\Delta t^2]$ | 0.025 | 0.073 |
| $rms_a\ [px/\Delta t^2]$ | 0.04 | 0.087 |
| DAR | 23 | 10 |

acceleration range (DAR). The values of velocity and acceleration errors attained by the STB at the last iteration are summarized in Table 3; the values of the dynamic ranges are comparable to the ones indicated by Schanz et al (2016) concerning time-resolved data.
The performances of the iterative STB approach in terms of fraction of detected tracks and velocity and acceleration errors suggest the suitability of multi-pulse systems in providing access to the measurement of the material acceleration, in particular when a variable time separation between the pulses is adopted to increase the dynamic range of the measure.

## 4. Conclusions and outlook

A performance assessment of the iterative STB approach for multi-pulse data proposed by Novara et al (2015) is carried out by means of the analysis of two synthetic experiments.
Particle images as acquired from virtual multi-pulse acquisition systems are generated based on the velocity fields resulting from numerical simulations. The availability of the ground-truth particle and flow fields allows for the evaluation of the number of actual particles identified by STB and for the quantification of the measurement errors in terms of position, velocity and material acceleration. The effect of the main experimental (seeding density, image noise, time separation) and processing parameters (number of STB iterations, IPR and particle tracking settings) is investigated.
Results from a DNS simulation of isotropic turbulence from the Johns Hopkins Turbulent Database are used to generate four-pulse images with a constant time separation; the image seeding density and noise levels are varied to simulate real experimental conditions.
Results show the capability of the iterative STB technique to identify most of the actual tracks even for the most challenging cases; the progressive reduction of the image density on the residual images allows to overcoming the limitations of 0.05 *ppp* reported for the reconstruction of single time instants alone. The comparison with Tomo-3D-PTV shows the higher particle peak location accuracy of the IPR when compared to MART tomographic reconstruction. The values of the position and velocity errors well compare with those indicated by Schanz et al (2016) for the time-resolved case. Nevertheless, the short observation time of the four-pulse approach does not allow for a significant reduction of the measurement noise by means of track fitting.
Aiming to increase the measurement dynamic range and to allow the extraction of the material acceleration, a synthetic four-pulse transonic base flow experiment has been generated in the framework of the NIOPLEX project, where a larger time delay is set between the second and

third pulse. The tracking algorithm within the STB is adapted to cope with the uneven pulse separation.

Results show that approximately 99% and 88% of the actual particles are retrieved by STB for the ideal image case and the noisy image case respectively. The fraction of four-pulse *ghost tracks* is lower than 1% even for the noisy case, suggesting that the longer observation time is sufficient to prevent *ghost* particle from being coherent with the flow motion even if a single imaging system only is used to record the four pulses.

The behavior of the position, velocity and acceleration errors shows that the application of further iterations of STB allows to the progressive identification of high curvature tracks exhibiting large acceleration within the shear layer region. As expected particle image noise results in larger error values; nevertheless, relatively high dynamic range values for both velocity and acceleration are achieved which compare well to those found by Schanz et al (2016) for the time-resolved case.

Results suggest the suitability of STB to analyze multi-pulse data for the measurement of the material acceleration, opening the possibility of accurate instantaneous pressure determination for high-speed flows.

As indicated by Novara et al (2015), the choice of the pulse separation strategy can affect the accuracy of the results; in particular the use of polarized light is suspected to result in large variation of the particle intensity along the track, ultimately causing loss of tracks. The detailed investigation of the effects of different pulse separation strategies by means of the analysis of experimental data is devoted to a future study.

## APPENDIX

### Particle-Space Correlation

During the tracking phase of STB the use of a velocity field as a predictor allows to reduce the search radius used for partner search, improving the identification of the particle tracks, in particular for the short recording sequence of multi-pulse experiments.

In order to obtain a velocity predictor field, a cross-correlation approach is deemed suitable due to its robustness to noise and *ghost* peaks. Several cross-correlation methods rely on the discretization of the domain into voxel elements. In Tomo-PIV the interrogation is performed between MART reconstructed objects where particles are represented by groups of voxel intensities; Pereira and Gharib (2002) proposed representing particle positions obtained from defocusing PIV as Gaussian blobs to perform cross-correlation in the 3D space.

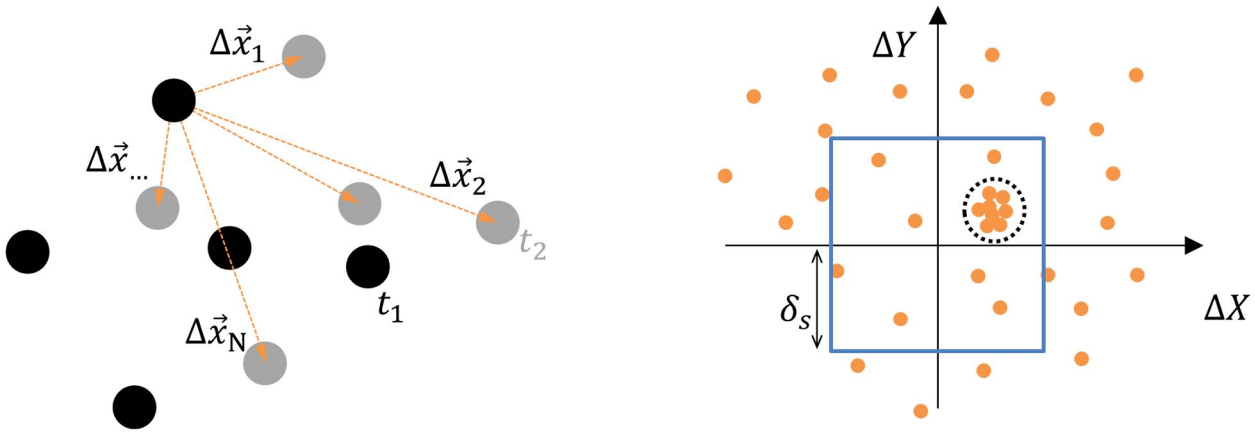


Figure 13. Two-dimensional sketch of the cross-correlation operated in the particle space. Left: particles within the interrogation volume at $t_1$ and $t_2$ (black and gray respectively). Right: map of the shifts in the $XY$ plane; $\delta_s$ indicates the search radius while the dashed black circle highlights the region of the most probable shift.

Due to the computational costs involved, the discretization of the investigated domain proves unpractical for the evaluation of instantaneous predictor fields.

Here on the other hand. A cross-correlation approach is introduced (Particle-Space Correlation), which solely relies on the representation of particles as triangulated by the IPR technique (points with position $\vec{x}$ and intensity $I$).

After IPR reconstruction of two pulses (e.g. $t_1$ and $t_2$), a Cartesian grid is defined within the 3D domain; for each grid point a spherical interrogation volume is applied, and the reconstructed particles within this region are identified at each time instant, Figure 13-left.

The shift between each particle at $t_1$ and all particles at $t_2$ is computed as:

$$\Delta\vec{x}_k = \vec{x}_j - \vec{x}_i \qquad 5$$

Where $j$ and $i$ loop over $M$ and $N$ (number of particles at $t_2$ and $t_1$ respectively). For each element in $\Delta\vec{x}$ the product of the particle peak intensity is evaluated as:

$$I_k^* = I_j \cdot I_i \qquad 6$$

The map of the shifts is presented in Figure 13-right where each shift is plotted as a point with coordinates $\Delta X, \Delta Y, \Delta Z$; if the particles within the interrogation volume exhibit a rather uniform displacement, the points in the map of the shifts cluster around the location of the most probable displacement.

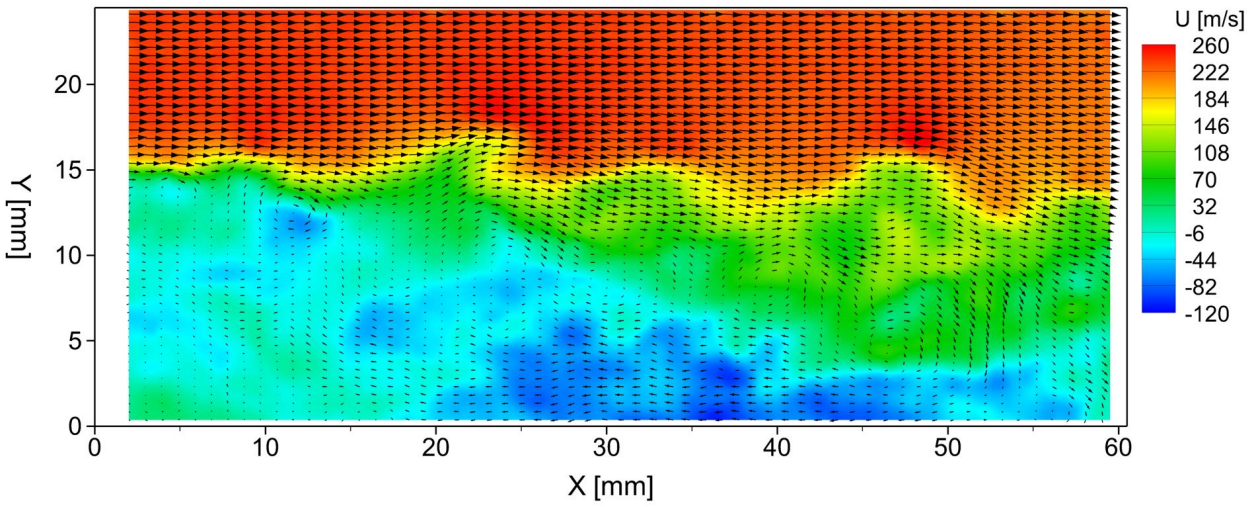


Figure 14. Contours of instantaneous stream-wise velocity component from Particle-Space Correlation of two subsequent pulses from the noisy case of the base flow synthetic experiment; the final correlation volume size is equivalent to 24×24×24 $px^3$ (50% overlap). Velocity vectors (4 and 2 vectors are skipped along $X$ and $Y$ for sake of clarity) and contours shown at $Z = -0.1\ mm$.

A search radius $\delta_s$ is chosen based on the expected maximum displacement (blue rectangle in Figure 13-right); a Gaussian blob having a peak value proportional to $I_k^*$ (typically of 3×3×3 elements) is positioned at each shift location (orange dots in Figure 13-right). The cross-correlation map is obtained adding the Gaussian blobs; when enough particles are found within the interrogation volume, a peak forms in the correlation map.

As for typical PIV evaluations, a Gaussian fit of the correlation coefficient is applied to retrieve the position of the peak and therefore the three components of the velocity vector.

For each grid point, only the region defined by the search radius is discretized, which largely reduces the computational effort when compared to voxel based methods. The spatial resolution of the discretization can be freely chosen in order to balance the computational effort and the accuracy of the correlation peak detection.

An iterative procedure analogous to that proposed for the volume deformation iterative multigrid cross-correlation technique (VODIM, Scarano and Poelma 2009) can be applied to progressively increase the spatial resolution. The volume deformation is applied simply by shifting the particle locations according to the previously estimated velocity field, resulting in a significantly lower computational burden when compared to cross-correlation approaches performed in the voxel space. Moreover, the search radius is progressively reduced after the first iteration, which further reduces the computational cost.

The technique has been successfully employed to evaluate velocity predictor fields used for STB processing of the base flow synthetic images; an example of the stream-wise velocity component is shown in Figure 14 relative to the noisy case (final cross-correlation size equivalent to $24\times24\times24\ px$).

Results compare well with those obtained from Tomo-PIV processing of the same particle images with similar grid refinement strategy and resolution (10 SMART iteration followed by 3D direct cross-correlation as implemented in LaVision Davis 8.2).

A comparable computation time of approximately 3 minutes for one instantaneous velocity field is reported using a single-core in-house Matlab implementation of the Particle-Space correlation method and for the cross-correlation of two volumes reconstructed by MART on a twenty cores server (2×Xeon E5-2680 quad core CPUs) with LaVision Davis 8.2. Regarding the latter case, the MART reconstruction time is not taken into account.

Considering the potential in terms of implementation optimization, the Particle-Space correlation could prove a powerful tool to obtain 3D velocity field from 3D particle triangulation approaches (such as IPR) both within the STB processing and as a stand-alone interrogation technique.

The fact that each particle pair contributing to the correlation peak can be identified within the interrogation volume opens the possibility of adapting the choice of the tracers to be considered for the motion analysis based on the velocity spatial gradients (similarly to what proposed by Novara et al 2013) effectively improving the spatial resolution. Furthermore, this feature could be exploited within the STB iterative approach to improve the robustness of the reconstruction and tracking process.

**Acknowledgements**

The NIOPLEX consortium is kindly acknowledged for providing the transonic base flow synthetic experiment. The authors thank Paul Blinde and Dirk Michaelis for the assistance and feedback concerning the reference data.

**References**

Adrian R J (1997) Dynamic ranges of velocity and spatial resolution of particle image velocimetry. Meas Sci Technol 8:1393-1398

Atkinson C and Soria J (2009) "An efficient simultaneous reconstruction technique for tomographic particle image velocimetry" Exp Fluids 47 pp 563-578

Blinde P, Michaelis D, van Oudheusden B, Weiss PE, de Kat R, Laskari A, Jeon YJ, David L, Schanz D, Huhn F, Gesemann S, Novara M, McPhaden C, Neeteson N, Rival D, Schneiders JFG and Schrijer F (2016) "Comparative assessment of PIV-based pressure evaluation techniques applied to a transonic base flow", 18th Int Symp on the Application of Laser Techniques to Fluid Mechanics, July 4-7, Lisbon, Portugal

Cao NZ and Chen SY (1999) "Statistics and structures of pressure in isotropic turbulence" Phys Fluids 11 pp 2235-2250

Deck S (2005) Zonal-Detached-Eddy Simulation of the Flow Around a High-Lift Configuration. AIAA J 43:2372–2384. doi: 10.2514/1.16810

Deck S (2012) Recent improvements in the Zonal Detached Eddy Simulation (ZDES) formulation. Theor Comput Fluid Dyn 26:523–550. doi: 10.1007/s00162-011-0240-z

Discetti S, Ianiro A, Astarita T and Cardone G (2013) "On a novel low cost high accuracy experimental setup for tomographic particle image velocimetry" Meas Sci Technol 24 075302

Elsinga GE, Scarano F, Wieneke B and van Oudheusden BW (2006) "Tomographic particle image velocimetry" Exp Fluids 41 pp 933-947

Elsinga GE, Westerweel J, Scarano F and Novara M (2011) "On the velocity of ghost particles and the bias error in Tomographic-PIV" Exp Fluids 50 pp 825-838

Gesemann S, Huhn F, Schanz D and Schröder A (2016) "From Noisy Particle Tracks to Velocity, Acceleration and Pressure Fields using B-splines and Penalties", 18th Int Symp on the Application of Laser Techniques to Fluid Mechanics, July 4-7, Lisbon, Portugal

Herman GT and Lent A (1976) "Iterative reconstruction algorithms" Comput Biol Med 6 pp 273-294

Huhn F, Schanz D, Gesemann S, Schröder A (2015) Pressure fields from high-resolution time-resolved particle tracking velocimetry in 3D turbulent flows, Proc. NIM2015 Workshop, Poitiers, France, 2015

Kähler CJ and Kompenhans J (2000) "Fundamentals of multiple plane stereo particle image velocimetry" Exp. Fluids 29 S70-7

Kähler CJ, Scharnowski S and Cierpka C (2012a) "On the uncertainty of digital PIV and PTV near walls" Exp Fluids 52 pp 1641-1656

Kähler CJ, Scharnowski S and Cierpka C (2012b) "On the resolution limit of digital PIV" Exp Fluids 52 pp 1629-1639

Lynch KP and Scarano F (2014) "Material acceleration estimation by four-pulse Tomo-PIV" Meas Sci Technol 25 084005

Lynch KP and Scarano F (2015) "An efficient and accurate approach to MTE-MART for time-resolved tomographic PIV" Exp Fluids 56:66

Novara M and Scarano F (2013) "A particle-tracking approach for accurate material derivative measurements with tomographic PIV" Exp Fluids 54:1584

Novara M, Schanz D, Kähler CJ and Schröder A (2015) "Shake-The-Box for multi-pulse tomographic systems: towards high seeding density particle tracking in high speed flows" 11th Symp PIV Santa Barbara, CA, US

Pereira F and Gharib M (2002) "Defocusing digital particle image velocimetry and the three-dimensional characterization of two-phase flows" Meas Sci Technol 13 pp 683-694

Scarano F and Poelma C (2009) "Three-dimensional vorticity patterns of cylinder wakes" Exp. Fluids 47 69–83

Schanz D, Gesemann S and Schröder A (2016) "Shake-The-Box: Lagrangian particle tracking at high particle image densities" Exp In Fluids 57:70

Schanz D, Gesemann S, Schröder A, Wieneke B and Novara M (2013) "Non-uniform optical transfer function in particle imaging: calibration and application to tomographic reconstruction" Meas Sci Technol 24 024009

Schanz D, Schröder A, Gesemann S, Michaelis D and Wieneke B (2013) "Shake-the-Box: a highly efficient and accurate Tomographic Particle Tracking Velocimetry (TOMO-PTV) method using prediction of particle position" 10th Symp PIV Delft, The Netherlands

Schröder A, Schanz D, Geisler R, Willert C and Michaelis D (2013) "Dual-volume and four-pulse Tomo-PIV using polarized light" 10th Symp PIV, Delft, The Netherlands

Van Oudheusden BW (2013) "PIV-based pressure measurement" Meas Sci Technol 24 032001

Wieneke B (2008) "Volume self-calibration for 3D particle image velocimetry" Exp Fluids 45 pp 549-556

Wieneke B (2013) "Iterative reconstruction of volumetric particle distribution" Meas Sci Technol 24 024008